Dept. of Mech. Eng.
CUET

Published Online April 2017 (http://www.cuet.ac.bd/merj/index.html)

Mechanical Engineering Research Journal

Vol. 10, pp. 57-65, 2016

ISSN: 1990-5491

NUMERICAL ANALYSIS ON PROPERTIES OF LARGER VOLUME MICRODISCHARGE GENERATED IN AN EXPERIMENTAL INVESTIGATION FOR MICROPLASMA REACTOR

R. K. Das[1*] and Shin Jichul[2]

[1]Department of Mechanical Engineering, Chittagong University of Engineering and Technology, Chittagong-4349, Bangladesh.
[2]School of Mechanical Engineering, University of Ulsan, Ulsan, 680-749, South Korea

Abstract: Micro plasma reactor technology either for fuel reforming or material processing is based on using the energy of the high temperature electrons and other charged particles. Microhollow cathode sustained discharge (MCSD) is a particular type of microdischarges configuration that uses microhollow cathode discharge (MHCD) as an electron source for sustaining larger volume plasma. This enlarged volume microplasma serve as a source of high temperature electrons, ions and other excited species. At high gas pressure, microdischarges in these specific geometries possess several unique properties that can be very stable and useful tools for atomic emission spectrometry, surface treatment and reduction of pollutants, fuel reforming and generation of UV radiation. Limitation of experimental data in conventional diagnostics due to small dimension, a detailed study on this microdischarge relies on numerical analysis. In this study a combined simulation of the MCSD and the MHCD is attempted and the corresponding simulation results of discharge properties such as electrostatic potential, electron density, atomic and molecular ion densities, excited species (metastables) densities, electron temperature, gas temperature, etc. are presented. The glow discharge model is based on a self-consistent, multi-species, continuum (fluid) model which describes the microdischarge phenomena by solving conservation equations for plasma species continuity and electron energy, and Poisson's equation for the self-consistent electric field. The expansion of microdischarges in the sustained discharge region does not noticeably alter the characteristics of the MHCD. The influences of gas pressure on sustained discharge properties are also investigated. Predictions from numerical simulations are compared with experimental investigation. It is found that ions are responsible for plasma expansion at lower pressure in the sustained discharge with positively biased third electrode observed in the experiment.

Keywords: *Discharge Properties, Fluid Model, Glow Discharge, MHCD, MCSD.*

1. INTRODUCTION

Plasma, often termed the fourth state of matter, is an ionized gas consisting of positively and negatively charged particles with some unique properties to distinguish it from three other states, solid, liquid and gases. Interestingly, much of the visible matter in the universe, viz., stars, all visible interstellar matter, is in the plasma state comprising 99% of the universe, both by mass and by volume. Since it first discovery by Sir William Crookes in 1879 [1], plasma has been produced in a variety of discharge configuration with different mechanism including dielectric barrier (DBD) discharge, microwave discharge, radio frequency (RF) discharge, direct current (DC) glow discharge etc. These plasma discharges shows collective behavior creating a highly reactive environment that contains charged particles, excited species, and radicals. The ionization degree of plasma discharges can vary from 100% (fully ionized gases) to very low values (e.g. 10^{-4}–10^{-6}; partially ionized gases). In a laboratory, one of the simplest ways to produce plasma is applying an electric field to a neutral gas. Microdischarges are

* **Corresponding author:** Email: ratanme06_cuet@yahoo.com

being developed to answer the increased interest in generating stable non thermal plasma at high gas pressure. One such discharge configuration is the microhollow cathode discharge (MHCD) [12], which is a glow discharge consisting of two parallel electrodes, one anode and another cathode, separated by an insulator with a center cylindrical hole. High pressure operations with larger surface to volume ratios make them useful in various applications from photonic device [2] to biomedical treatment [3]. However, due to limited volume of MHCDs, practical applications are still limited. Limited volume of MHCD is expanded placing another electrode outside the MHCD hole [4],which pulls the electrons toward the third electrode and form discharge in between MHCD and electrode called microhollow cathode sustained discharge (MCSD). A schematic diagram of such configuration is shown in Fig. 1.

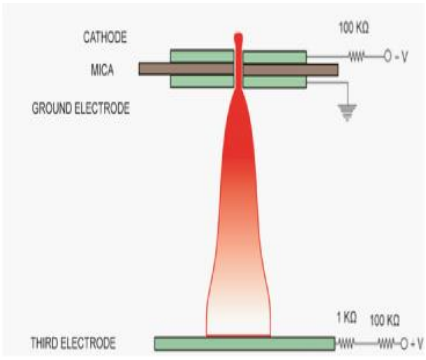

Fig. 1 Schematic diagram of microhollow cathode sustained discharge (MCSD).

Here MHCD has been utilized as cathode which behaves as an electron source for generating a stable diffuse discharge which extends from the microhollow cathode to third positively biased electrode. Some application of MCSD has been reported like micro reactor for singlet oxygen generation [5], plasma sources of singlet delta oxygen (SDO) for biomedical application [6], DNA oxidization [7] etc. As a microplasma reactor either for fuel reforming or material processing microdischarges serves as sources of high energy electrons, ions and radicals. A good insight providing details description of glow discharge would be an important step to improve the results in all this application fields. However, the reduced dimension makes conventional diagnostic of microplasma for experimental characterization very complicated and challenging. As a result, a detailed study on the MHCD or the MCSD relies on numerical simulations [8~9]. Recently a numerical simulation on the MCSD is performed by Serrano *et al* [9] by treating the MHCD as an electron source and treating quasi neutral plasma in the sustained discharge between the MHCD and the third electrode. It is reported that the MCSD is nothing but a positive column expanded by a weak electric field in the presence of third electrode. However, they didn't mention details of gas temperature and electron temperature profiles in their studies which are also crucial parameter for some application such as microchemical reactor [10]. Moreover, in their studies the information on the sustained discharge is not adequate. Better information, such as plasma species responsible for volume expansion in the sustained discharge, is expected as MCSD is more important than MHCD for their potentiality due to expanded plasma volume. In order to provide more detailed information on the MCSD, a numerical simulation of the MHCD and The MCSD is attempted simultaneously and compared with experimental observation in this article.

2. METHODOLOGY

Numerical simulation of non-equilibrium glow discharge plasma of the MCSD is performed with VizGlow plasma modeling tool [17]. The model is based on 2-D axis-symmetric, self-consistent, continuum fluid description of the plasma. Table 1 show the high-pressure argon plasma gas-phase chemistry used in this model

Table 1 High-pressure argon plasma gas-phase chemistry used in this model

#	Reactions	Reaction rate	Ref.
G_1	e + Ar => e + Ar	b)	58
G_2	e + Ar => e + Ar*	b)	58
G_3	e + Ar => 2e + Ar^+	b)	58
G_4	e +Ar* => 2e + Ar^+	b)	58
G_5	e + Ar* => e + Ar	b)	58
G_6	e + Ar+ => Ar*	$4.0\times10^{-13}T_e^{-0.5}$	62
G_7	2e + Ar+ => Ar* +e	$5.0\times10^{-8}T_e^{-4.7}$ $cm^6.s^{-1}$	62
G_8	e + Ar_2+ => Ar* +Ar	$5.38\times10^{-8}T_e^{-0.66}$	62
G_9	2Ar* => Ar^+ + Ar +e	5.0×10^{-10}	62
G_{10}	$2Ar_2^*$ => Ar_2^+ + 2Ar +e	5.0×10^{-10}	62
G_{11}	Ar* + 2Ar => Ar_2^* + Ar	1.14×10^{-32} $cm^6.s^{-1}$	62
G_{12}	Ar^+ + 2Ar => Ar_2^+ + Ar	2.5×10^{-31} $cm^6.s^{-1}$	62
G_{13}	Ar_2^* => 2Ar	$6.0\times10^7 s^{-1}$	62
G_{14}	e + Ar2* => 2e + Ar_2+	$9\times10^{-88}T_e^{0.7}$ $\exp(-3.66/T_e)$	62
G_{15}	e + Ar2* => e + 2Ar	10^{-7}	62

[a]Rate coefficients have units of cm^3s^{-1}, unless mentioned otherwise. The electron temperature, T_e, is in Kelvin

[b]Tabulated rate coefficient as a function of mean electron temperature was obtained by the Boltzmann equation solver "BOLSIG+" [16].

Species conservation, electron energy and gas energy equations are solved in the gas sub domain, while Poisson's equation for electrostatic potential is solved in the gas and in the dielectrics sub domain. MCSD is generated in argon at a pressure 60 Torr and 300 Torr using MHCD as an electron source. The argon species involved in the simulation includes electron (e), ions (AR^+, AR_2^+) and metastable (AR^m). As shown in Fig. 2, MHCD includes five layers in order to avoid the undesired expansion of the discharges over bottom surface near the MHCD hole. The MHCD hole diameter is 300 μm. The thickness of each electrode and dielectric is 0.2mm and the third electrode is placed at a distance of 3mm from the MHCD hole. Total current through third electrode is similar to 3mA at 60 Torr and 10 mA at 300 Torr. In order to provide a uniform

distribution over the entire electrode a ballast resistor is connected to third electrode. To obtain a stable numerical solution first the MHCD is run with a time step of $5X10^{-12}$s until a steady state is reached with third electrode turned off.

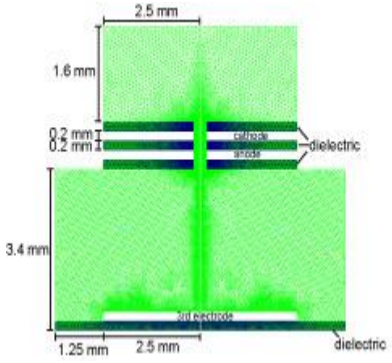

Fig. 2 Computational mesh of MHCD and MCSD. The geometry is cylindrically symmetric.

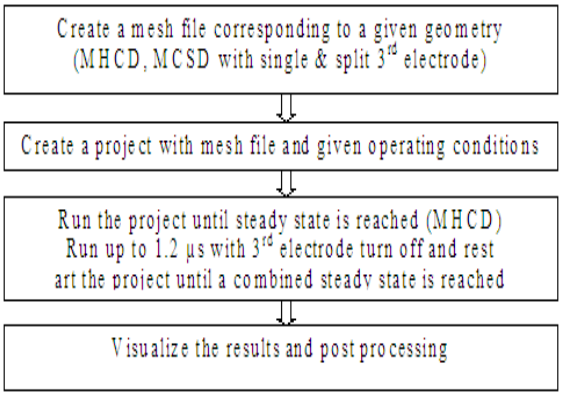

Fig. 3 Roadmap of the Simulation Process.

Then the third electrode is turned on and simulation is restarted at 1.2 μs with a smaller time step of $5X10^{-12}$s which is found to be necessary to reach a combined steady state for the MHCD and MCSD. The simulation is run on 16 processors. Total number of cells in the mesh is 25,811. In all cases, a combination triangles and quadrilaterals cells is used in the plasma region. Farfield boundaries on the gas sub domain of the discharge are modeled as floating circuit for poison's equation and solid surface flux for other equations to avoid secondary discharges between electrode and outer boundaries. Backward Euler scheme for temporal discretization and an upwind scheme for spatial discretization of the governing equations have been implemented. The equations are marched forward in time from a specified initial state. A variety of acceleration techniques is used to speed up convergence of the numerical solution to the steady state. Corresponding variable is updated by a certain time step. The problem specification is divided into three distinct stages 1) specification of geometry and meshing of the geometry, 2) specification of materials definitions (gas and multiple surface phase definitions), and 3) specification of the plasma problem itself. Road map of the simulation is discussed below:
First step is to create a mesh file corresponding to a given geometry (MHCD and MCSD) using VizMesh2D [17]. The next step is to create a project file with this mesh file and given operating conditions using OverViz Graphical User Interface [17]. Then the project is run and result is visualized (Fig. 3).

2.1 GOVERNING EQUATIONS

2.1.1 Species continuity

The densities of individual species in the discharge are determined by the species continuity equation,

$$\frac{\partial n_k}{\partial t} + \vec{\nabla}.\vec{f}_k = \dot{G}_k + \frac{\left(n_k^{in} - n_k\right)}{\tau_{flow}}, \quad \text{k=1……, Kg} \qquad (1)$$

Where n_k is the number density of species of index k (units: #/m^3-s), $\vec{f}_k$ is the total species k number flux density (unit, $\vec{G}_k$ is the gas-phase species generation rate through plasma chemical s: #/m^2-s), and K_g is the total number of gas-phase species. The right hand side of Eq. (1) comprises the number density source term $\dot{G}_k$ due to gas-phase chemical regions and the second term is an optional source term due to bulk flow residence time effects that may exist in the discharge. The inlet densities are typically assumed non-zero for species in a feed gas to the discharge. The dominant neutral species is identified as the "background" species; its density being determined to satisfy the ideal gas law,

$$p = \sum_{k=1}^{k_g} n_k k_B T \qquad (2)$$

Where k_B=1.3807×10^{-23} J/K is the Boltzmann's constant and T_k is the species temperature and p is the system pressure. The number density of dominant background species is therefore given as

$$n_d = \frac{p - \sum_{k=1, k\neq k_d}^{K_g} n_k k_B T_k}{k_B T_d} \qquad (3)$$

Where n_d is the number density, T_d is the temperature, and k_d is the species index of the dominant background species. A relaxation factor ζ_{igeos} is imposed so that updates to n_d from each subsequent step is relaxed, i.e. the new update $n_d^{new} = n_d^{old} + \zeta_{igeos}\left(n_d - n_d^{old}\right)$. The value of ζ_{igeos}=1 is used in this study.

2.1.2 Electron energy

The electron temperature, T_e, is determined by solution of the electron energy equation which is given as follows.

$$\frac{\partial e_e}{\partial t} + \vec{\nabla}.\{(e_e + p_e)\vec{u}_e + \vec{q}_e\} = S_e, \qquad (4)$$

Where $e_e = \left(\frac{3}{2}k_b T_e + \frac{1}{2}m_e u_e^2\right)n_e \approx \frac{3}{2}k_B T_e n_e$ is the electron volumetric energy (units: J/m^3) which includes the contribution from the electron thermal and electron fluid kinetic energies, but is approximately equal to electron thermal energy since $T_e >> m_e u_e^2 / k_B$ is a non-equilibrium plasma. $p_e = n_e k_B T_e$ is the electron pressure, $\vec{u}_e = \vec{u} + \vec{U}_e$ is the electron total fluid velocity, and $\vec{q}_e = -\kappa_e \vec{\nabla} T_e$ is the electron thermal flux (units: J/m^2-s). It is also convenient to define the total electron energy flux $\vec{Q}_e = (e_e + p_e)\vec{u}_e + \vec{q}_e$, a term that will be used later. The source term on the right hand side of the equation is given by

$$S_e = \xi_{ejh}\vec{j}_e.\vec{E} - e\sum_{i=1}^{I_g}\Delta E_i^e r_i - \frac{3}{2}k_B n_e\left(\frac{2m_e}{m_b}\right)(T_e - T_g)\bar{\nu}_e - \frac{e_e}{\tau_{flow}} + P_e^{ext} \quad (5)$$

Where, the first term is the electron Joule heating term with, $\vec{j}_e = -e\vec{f}_e$ being the electron total current density (units: A/m^2). $\xi_{ejh} = 1$, is used to specify a non-unity contribution of the electron Joule heating term to electron energy equation. The second term on the right hand side is the contribution of the inelastic collision terms to the electron energy, where ΔE_i^e is the inelastic collisional energy lost by an electron per collision event as described by the chemical reaction i (units: eV, positive for energy lost by an electron), r_i is the rate of progress of the chemical reaction, and I_g is the total number of gas-phase reactions. The third term is the contribution due to elastic collisional loss of electrons with the heavy species, where T_g is the heavy species (gas) temperature, m_e is the electron particle mass, m_b is the background (heavy) species particle mass, and $\vec{\nu}_e$ is the electron momentum-transfer collision frequency with the background. The forth term is the electron energy lost due to bulk flow. Finally, the last term on the right hand side P_e^{ext} is the external power input into the electrons.

2.1.3 Electrostatic Potential

The self-consistent electrostatic potential in the discharge is determined by solving the Gauss' law (part of the Maxwell's equation set). For non-equilibrium discharge conditions is often possible to neglect the effects of induced magnetic fields (due to relatively weak plasma conduction and displacement currents) and solve only for the electrostatic fields using a subset of the Maxwell's equation, i.e. the Gauss' law. Electrostatic fields are typically driven by voltage biased surfaces in the discharge. For non-zero space charge, Gauss' law takes the form of Poisson's equation given as

$$\nabla.(\varepsilon_r \nabla\Phi) = -\frac{\rho_c}{\varepsilon_o}, \quad (6)$$

Where ε_r is the relative dielectric permittivity of the material (here =1 for gas), ρ_c is the space charge density (units: C/m^3), and ε_o is the dielectric permittivity of vacuum (8.854×10^{-12} F/m). The space charge density in the gas is determined as

$$\rho_c = e\sum_{k=1}^{K_g} Z_k n_k \quad (7)$$

Where Z_k is the species charge number (e.g. -1 for electrons, +1 for single charge positive ion)

2.1.4 Species momentum

We use drift-diffusion approximation for neutral species and electrons and use separate species momentum equations for all ions. The need for solving the full ion momentum equation for ions arises in low pressure discharge (p<100's mTorr) [18] or in small-scale microdischarge despite the high pressures [19]. In these situations the strong electric fields in the sheath regions or double layer effects must be explicitly included by solving the ion momentum equation. The ion number flux densities are evaluated as $\vec{\Gamma}_i = n_i\vec{u}_i$, where $\vec{u}_i$ is the ion fluid velocity, which is determined using the first moment of the ion species Boltzmann equation, i.e., the ion species momentum equation,

$$\frac{\partial n_i\vec{u}_i}{\partial t} + \vec{\nabla}.(n_i\vec{u}_i\vec{u}_i) = -\frac{eZ_i}{m_i}n_i\vec{E} - \frac{1}{m_i}\vec{\nabla}p_i - n_i(\vec{u}_i - \vec{u})\bar{\nu}_i \quad (8)$$

Where n_i is the ion number density, m_i is the ion particle mass, $\bar{\nu}_i$ is the ion species collision frequency, Z_i is the ion charge number, e is unit charge (1.602×10^{-19}C), $\vec{E}$ is the electric field, $p_i = n_i k_B T_i$ is the ion species pressure, and $\vec{u}_i$ is the mean mass fluid flow velocity. The ion temperature is given by T_i. For weak driving fields the ion temperature is the same as the background gas temperature. However, for moderate to strong fields the ion temperature is an effective ion temperature determined by sum of the thermal energy and the drift energy derived from the fields. To be consistent with the drift-diffusion formulation, the ion temperature is obtained by the ratio of the ion diffusion co-efficient and the ion mobility, i.e. the characteristics temperature of the ions given as,

$$T_i = T_{effi} = \left(\frac{Z_i e}{k_B}\right)\frac{D_i}{\mu_i} \quad (9)$$

Here Z_i is the ion charge number; D_i is the ion diffusion co-efficient and μ_i is the ion diffusion coefficient as determined by the transport formulation discussed in.

The large thermal energy of electrons guarantees validity of drift-diffusion approximation for electrons even in high field regions of the discharge. The neutral species are obviously not affected by electric fields and hence the drift-diffusion approximation remains valid for neutrals. The species total number flux density is defined as

$$\vec{f}_k = n_k \vec{u}_k = n_k\left(\vec{u} + \vec{U}_k\right) = n_k \vec{u} + \vec{\Gamma}_k \tag{10}$$

Where, $\vec{u}_k$ is the species k fluid velocity, $\vec{u}$ is the mean-mass bulk flow velocity, and $\vec{U}_k$ is species k drift-diffusive velocity, and $\vec{\Gamma}_k = n_k \vec{U}_k$ is the species drift-diffusion number flux.

2.2 Boundary Conditions

Boundary conditions for the governing equations discussed in the previous section are as follows:

2.2.1 Species continuity boundary equation

For solid surfaces, assuming that electrons are in equilibrium at temperature T_e near the wall, the net number flux of electrons from the discharge towards the wall can be written as

$$\vec{f}_e.n_e = \frac{1}{4} n_e \left(\frac{8k_B T_e}{\pi m_e}\right)^{1/2} - \sum_k \gamma_k f_k^{s+} \tag{11}$$

Where γ_k is the secondary electron emission coefficient of species k, and f_k^{s+} is the flux of all species k directed towards the wall. $\hat{n}_s$ is the outward unit vector normal to the surface. For ions,

$$\vec{f}_i.\hat{n}_s = f_i^{s+} = \frac{1}{4} n_i \left(\frac{8k_B T_g}{\pi m_i}\right)^{1/2} + n_i \max\left(0, -\mu_i \hat{n}_s.\vec{\nabla}\Phi\right) \tag{12}$$

And for neutrals,

$$\vec{f}_n.\hat{n}_s = f_n^{s+} = \frac{1}{4} n_n \left(\frac{8k_B T_g}{\pi m_n}\right)^{1/2} \tag{13}$$

In Eq. (12) and (13) we have made the implicit assumption that all heavy species have the same gas temperature Tg. The second term in Eq. (12) represents the mobility-limited flux for ions. In the case of positive ions, if the electric field is directed towards the wall, the mobility-limited flux term is positive, i.e. positive ions drift towards the wall. For negative ions, an electric field directed towards the surface keeps negative ions from drifting to the wall, resulting in a zero negative ion drift flux to the wall. The plasma model includes the capability of modeling surface reactions, and so the sign of the net flux of ions and neutrals to the wall depends on the surface chemistry. For the glow discharges studied in this work, neutral species are produced by surface recombination of ions and hence the net flux of neutrals towards a solid surface is negative.

For symmetry boundaries, the fluxes of all species k normal to the boundary are set to zero, i.e.

$$\vec{f}_k.\hat{n}_s = 0 \tag{14}$$

The axis boundary condition has the same meaning in the context of the species density equation as the symmetry boundary condition. The axis boundary condition is reserved for specification of boundary condition at the coordinate axis of a 2D axisymmetric problem. The axis boundary condition imposes a zero number flux of species normal to the boundary, i.e. $\vec{f}_k.\hat{n}_s = 0$.

2.2.2 Electric potential boundary condition

At electrode surfaces, the potential is usually specified as a constant or calculated implicitly if an external circuit is present. The potential on dielectric surfaces is determined using the total surface charge density accumulated on the surface. The equation for evolution of net surface charge density is given by

$$\frac{\partial \rho_s}{\partial t} = \sum_{k=1}^{k_g} e Z_k \vec{\Gamma}_k.\hat{n} \tag{15}$$

Where, ρ_s is the surface charge density. Based on surface charge density, Gauss's law can be used to compute the potential on dielectric surfaces. The anode surface is held at a ground potential, while an external circuit comprising a ballast resistor is inserted between the supply voltage and the cathode surface.

2.2.3 Electron Temperature

For the electron energy equation, the following energy flux is imposed at solid walls:

$$Q_e^w = \frac{5}{2} k_B T_e \Gamma_e^w \tag{16}$$

Where, Γ_e^w is the electron wall number flux. The gas temperature is fixed at 300 K at solid walls although slip temperature boundary conditions may require for smaller MHCD dimension.

2.2.4 Far-Field Boundaries

Far-field boundaries are defined as boundaries that are sufficiently far away from the primary discharge activity. Consequently far-field boundaries do not pass a net electrical current. Far-field boundaries are implemented as symmetry for electrostatic potential, species density, electron energy and bulk energy equation boundary condition for MHCD. For MCSD, far-field boundaries are set as floating circuit for external circuit equation and implemented as floating circuit for electrostatic potential equation and solid surface flux for other equations boundary condition.

2.2.5 External Circuit

The external circuit boundary condition is available for the solution of the electrostatic potential (Poisson's) equation.

3. PLASMA CHEMISTRY

A pure argon plasma gas chemistry is used and comprises six species: electrons (e), atomic argon ions (AR^+), molecular

argon ions (AR_2^+), metastable atoms (AR^m),dimer metastable atoms (AR_2^m), and the background argon atoms (AR). The reactions considered in the study comprises electron impact ionization and excitation reactions, Penning ionization reactions, three-body reactions for dimer excited species and ion formation, quenching and de-excitation reactions. At the surfaces all excited species and charged species are assumed to get quenched with unity sticking coefficient. Upon quenching at surfaces, each dimer ion and excited species is assumed to return to plasma a pair of ground state neutral AR atoms, while the monomer species return as a single AR atom.

4. RESULTS AND DISCUSSION

All spatial profiles presented here are axisymmetric and only for gas sub domain. Figs. 4-17 shows the spatial and axial distributions of potential, electron, ion and metastable population in the combined region of MHCD and MCSD. Left and right side of each figure represents numerical profiles at 60 Torr and 300 Torr respectively. The potential profile (Fig. 4) explains that MCSD is a positive column expanded outside the MHCD hole due to a weak electric field in the gap between MHCD and MCSD.

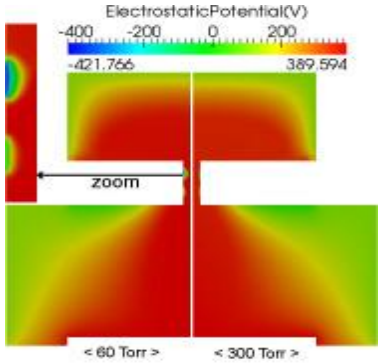

Fig. 4 Spatial profile of potential distribution.

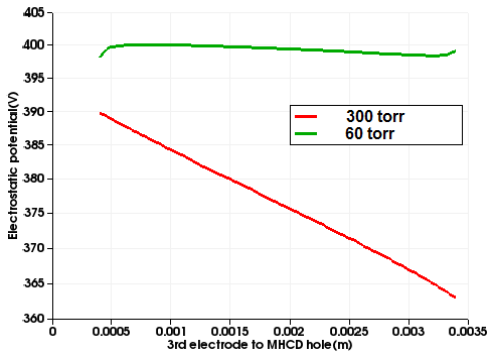

Fig. 5 Axial profile of potential distribution.

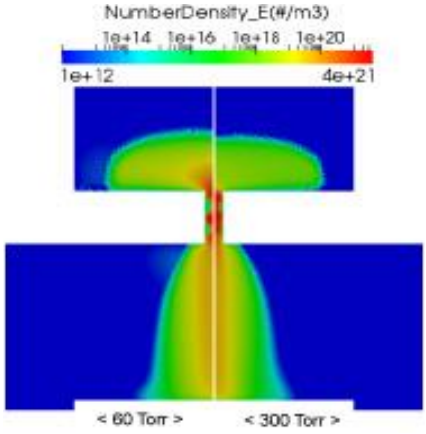

Fig. 6 Spatial profile of electron number density.

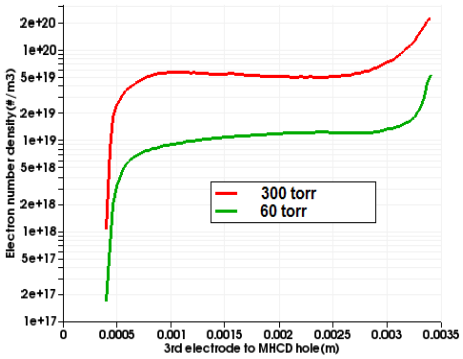

Fig. 7 Axial profile of electron number density.

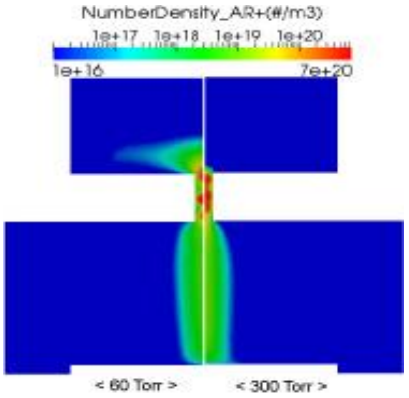

Fig. 8 Spatial profile of AR^+ number density.

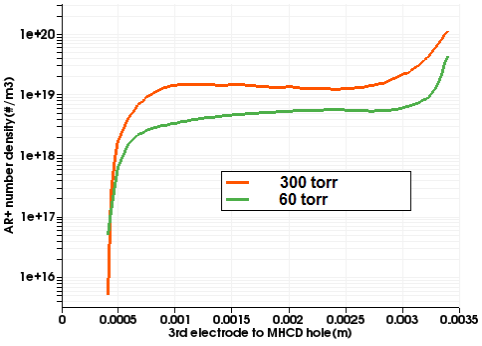

Fig. 9 Axial profile of AR^+ number density.

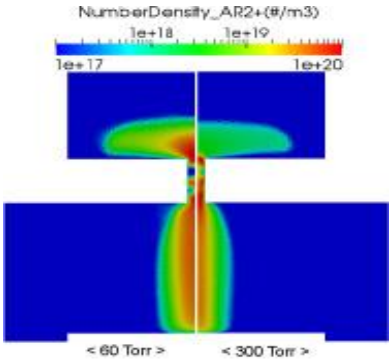

Fig. 10 Spatial profile of AR_2^+ number density.

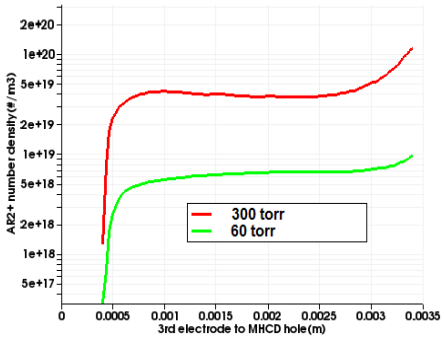

Fig. 11 Axial profile of AR_2^+ number density.

The MCSD volume looks quite dependent on the spatial distribution of electrons which is similar with the experiment (Fig. 18). The sheath area is confined inside the MHCD hole because of the dielectric layer on the top surface. Cathode sheath thickness reduced inside the microhole on the increase of gas pressure (300 Torr). Anode is also surrounded by a high sheath region and contributes to the supply of electrons for generating MCSD between the MHCD and third electrode both at 60 Torr and 300 Torr. As a result, whole MHCD act as cathode for the sustained discharge. The peak density is as high as $1x10^{20}$ m^{-3} at 60 Torr near the exit plane of MHCD and on-axis due to expansion of the plasma leaving the MHCD (Fig.6). While at 300 Torr the peak electron number density is $4x10^{21}$ m^{-3}. Electron densities in the mid plane of the sustained discharge are about 10^{17}-10^{18} #/m^{-3} which is in good agreement with the experimental result presented in Ref. [12]. In the MCS region, the peak monomer ion (AR^+) density is about ~$3x10^{19}$ m^{-3}, peak dimmer ion (AR_2^+) density is about ~10^{19} m^{-3}, peak value of metastable (AR^m) density is about ~$3x10^{20}$ m^{-3} occur along the exit hole of the MHCD on the centerline of the MCSD at 60 Torr. Peak values of plasma species are same or higher than other simulation result [4]. As shown in Fig. 6-17, when gas pressure is increased to 300 Torr, peak value of plasma species density also increases along the axis of the MCSD. Significant presence of excited species (AR^m) is useful in the sense that they are considered as important constituent for plasma assisted ignition. A region of constant density for all plasma species is observed on the central axis of the sustained discharge. Higher pressure favors three body conversion reactions (not shown) and reduces the loss of dimmer species due to surface quenching above the MHCD hole. As a result lifetime of dimmer ion is longer and the ratio of monomer to dimmer ion decreases outside the microhole at higher pressure (300 Torr) which support the similar observation in a numerical study of MHCD done by Deconinck *et al.* [13]. Peak values of electron, atomic ion, molecular ion and metastable particles number densities exceed $3x10^{20}$ m^{-3}, $2x10^{20}$ m^{-3}, $1x10^{21}$ m^{-3} and $2x10^{21}$ m^{-3} respectively at 300 Torr. At 60 Torr, peak value of bulk temperature (Fig. 14-15) is 1422K occurs along the centerline of the cathode region in the MHCD and negligible bulk temperature is observed in the MCSD. It shows consistency with the experiment in Ar/O_2 mixtures for measuring gas temperature in the MCS region [14]. Peak electron temperature (Fig. 16) is observed in the cathode sheath region within the hollow, which is in the order of several tens of eV. Other parts of the discharge maintain the electron temperature in the order of ~1 eV (Fig. 17). In an experimental observations in microdischarges [15], electron temperature is expected to be high, which support our results. At 300 Torr electron temperature remains unchanged but a slight increase in bulk temperature on the axis of the MCSD is observed while maintaining the peak temperature 2024K near cathode region of MHCD.

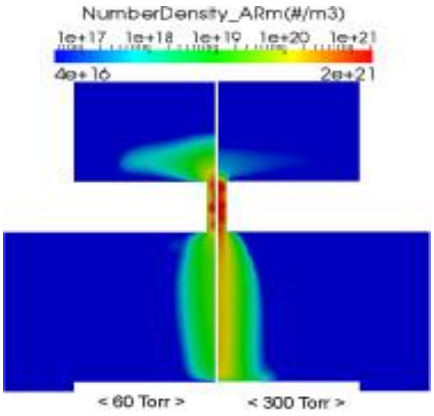

Fig. 12 Spatial profile of metastable (AR^m) number density.

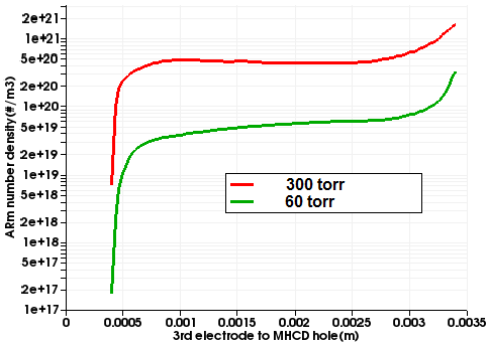

Fig. 13: Axial profile of metastable (AR^m) number density.

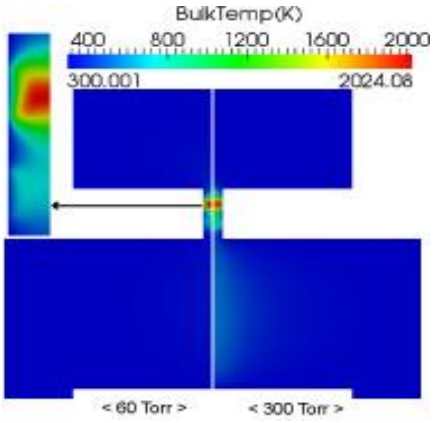

Fig. 14 Spatial profile of bulk temperature.

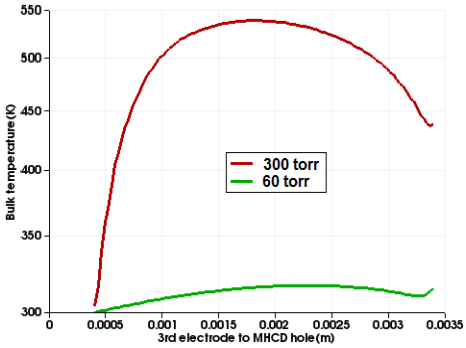

Fig. 15 Axial profile of bulk temperature.

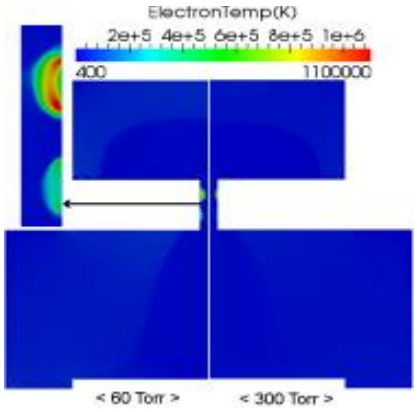

Fig. 16 Spatial profile of electron temperature.

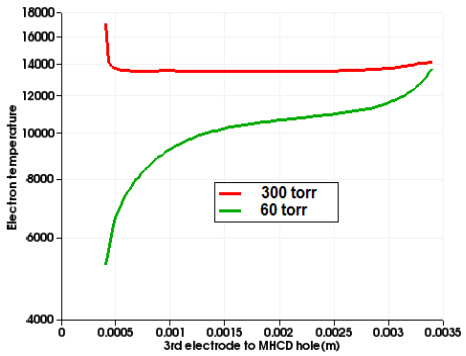

Fig. 17 Axial profile of electron temperature.

From experimental photo image (Fig. 18) it is seen that at 60 Torr plasma expansion in the sustained discharge is 3mm and at 300 Torr expansion is about 2mm. So at lower pressure plasma is more expanded than at higher pressure. From simulation it is observed that at higher pressure atomic and molecular ions are constricted while metastable species are comparatively expanded. However, electrons spatial distributions are more or less same at both pressures. So it can be declared that ions are responsible for plasma expansion at lower pressure in the sustained discharge. Here it is clear that expansion or constriction of plasma in the sustained region is depended on multiple species rather than one single species.

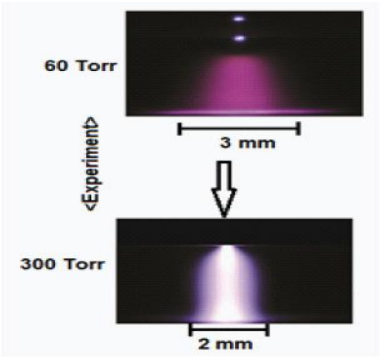

Fig. 18 Experimental photo image.

5. CONCLUSIONS

Mechanical behaviors of FSSW joints of two dissimilar ferrous alloys under opening-dominant combined loads were experimentally investigated. In this paper a two-dimensional axisymmetric, self-consistent, multispecies, multi-temperature, continuum (fluid) model is used to estimate different parameters like electrons, ions and metastable number density, bulk and electron temperature of microhollow cathode sustained discharge(MCSD). Charged species densities of order (10^{17}-10^{21}) #/m^{-3} and metastable species densities of order (10^{16}-10^{21}) #/m^{-3} are predicted for the condition investigated. Electron temperatures of several tens of eV near cathode sheath and ~1 eV in the remaining part of the discharge are predicted. The ions are found to be responsible for the volume expansion in the MCSD at lower pressure observed in the experiment.

REFERENCES

[1] W. Crooks, “Radiant matter, a resume of the principal ectures and papers”, Technical report, Royal Society of London and British Association for the Advancement of Science, James W. Queen & Co., 1879.

[2] S. -J. Park, J. G. Eden J. Chen and C. Liu, “Microdischarge devices with 10 or 30 mm square silicon cathode cavities:pd scaling and production of the XeOexcimer”, Appl. Phys. Lett., Vol. 85, No. 21, pp. 22, 2004.

[3] J. S. Sousa, G. Bauville, B. Lacour,V. Puech, M. Touzeau and J.-L. Ravanat, “DNA oxidation by singlet delta oxygen

produced by atmospheric pressure microdischarges", Applied Physics Letters, Vol. 97, 141502, 2010.

[4] K. Makasheva, G. J. M. Hagelaar, J. P. Boeuf, T. Callegari and L. C. Pitchford, "Ignition of microcathode sustained discharge," IEEE Trans. Plasma Sci., Vol. 36, pp. 1236–1237, 2008.

[5] J. S. Sousa, G. Bauville and V. Puech, "Arrays of microplasmas for the controlled production of tunable high fluxes of reactive oxygen species at atmospheric pressure", Plasma Sources Sci. Technol., Vol. 22, pp. 035012, 2013.

[6] J. S. Sousa and V. Puech, "Pressure Effects in the Spatial Development of Microcathode Sustained Discharges in Rare-Gas Oxygen Mixtures," IEEETrans. Plasma Sci., Vol. 39, 2011.

[7] J. S. Sousa, G. Bauville, B. Lacour,V. Puech, M. Touzeau and J.-L. Ravanat, "DNA oxidation by singlet delta oxygen produced by atmospheric pressure microdischarges", Applied Physics Letters, Vol. 97, pp. 141502, 2010.

[8] M. J. Kushner, "Modelling of microdischarge devices: plasma and gas dynamics," J. Phys. D: Appl. Phys., Vol. 38, no 4, pp. 1633-477, 2005.

[9] E. Munoz-Serrano, G. Hagelaar, Th. Callegari, J. P. Boeuf and L. C. Pitchford, "Properties of plasmas generated in microdischarges," Plasma Phys. Control. Fusion., Vol. 48, No. 12B, pp. B391–B397, 2006.

[10] R. M. Sankaran, "High pressure microdischarges as microreactors for materials applications", Ph.DThesis. California Institute of Technology, 2004.

[11] R. H. Stark and K. H. Schoenbach, "Direct current high-pressure glow discharges," J. Appl. Phys., Vol. 85, No. 4, pp. 2075–2080, 1999.

[12] T. Deconinck and L. L. Raja, "Modeling of Mode Transition Behavior in Argon Microhollow Cathode Discharges," Plasma Processes Polym., Vol. 6, No. 5, pp. 335-346, 2009.

[13] J. F. Lagrange, N. Sadeghi, M. Touzeau, G. Bauville, B. Lacour and V. Puech, "Gas temperature measurements in a microcathode sustained discharge in oxygen", Gaseous Electronics Conf (Columbus, Ohio, USA, October, 2006).

[14] C. Penache, M. Miclea, A. Brauning-Demian, O. Hohn, S. Schossler, T. Jahnke, K. Niemax and H. Schmidt-Bocking, "Characterization of a high-pressure microdischarge using diode laser atomic absorption spectroscopy", Plasma Sources Science and Technology, Vol. 11, pp. 476-483, 2003.

[15] G. J. M. Hagelaar and L. C. Pitchford, "Solving the Boltzmann equation to obtain electron transport coefficients and rate coefficients for fluid model", Plasma Sources Science and Technology, Vol. 14, pp. 722–733, 2005.

[16] See http://esgeetech.com/products/vizglow/ for VizGlow, 2013 Esgee Technologies.

[17] M. Meyyappan and J. P. Kreskovsky, "Glow discharge simulation through solutions to the moments of the Boltzmann transport equation", Journal of Applied Physics, Vol. 68, pp. 1506, 1990.

[18] T. Deconinck, S. Mahadevan and L. L. Raja, "Computational simulation of coupled nonequilibrium discharge and compressible flow phenomena in a micro plasma thruster",' Journal of Applied Physics, Vol. 106, 063305 pp.1-13, 2009.